Process flow model of solid oxide fuel cell system supplied with sewage biogas

J. Van herle[1], F. Maréchal[1], S. Leuenberger[1], Y. Membrez[2], O. Bucheli[3], D. Favrat[1]

[1]*Laboratory of Industrial Energy Systems (LENI), Faculty of Engineering, Federal Institute of Technology (EPFL), CH-1015 Lausanne, Switzerland,*

[2]*EREP SA, chemin du Coteau 9, CH-1123 Aclens, Switzerland,*

[3]*HTceramix SA, Science Park Ecublens (PSE), CH-1015 Lausanne, Switzerland*

Abstract

A model for a 100 kW class Solid Oxide Fuel Cell system running on biogas from a sewage sludge digestion plant was implemented in a process flow scheme using external steam reforming. The model stack consisted of planar anode supported cells operated at 800°C displaying state-of-the art electrochemical performance (0.15 W/cm^2 at 80% fuel utilisation). Real annual data from an existing sewage plant were used as input to the model. From the input of 43 m^3/h biogas (63% CH_4), equivalent to 269 kW (HHV), the SOFC stack was calculated to deliver 131 kW_e electricity (48.7%) using a steam-to-carbon ratio of 0.5. This would allow the sewage site to more than cover its own electrical needs, hence to depollute the waste stream at negative energy cost. In its current exploitation using a low efficient gas engine (130 kW), the site is only ≈50% self-sufficient. Special attention was given to the thermal balance of the stack. The stack developed heat (143 kW) could be balanced by endothermal reforming (78 kW) and by cathode excess air λ (=3) allowing a temperature difference between stack inlet and outlet of 200 K. The case was compared to other fuel scenarios. Steam-added biogas behaves basically identically to steam-reformed methane. For partial oxidation of biogas or pure hydrogen feeding, electrical efficiency drops to under 43% while λ needs to be raised to 4.5 respectively 6 to maintain the 200 K thermal gradient over the stack.

Keywords: biogas, SOFC system model, sewage sludge digestion, thermal balance of fuel cell stack, carbon deposition, composite curves

1. Introduction

Conversion of biogas to electricity presents an attractive niche application for fuel cells (1). Biogas production sites are small (of a few kW_{el} to few MW_{el}), plentiful (from sewage sludge, farm waste, landfill, industrial liquid waste, municipal and industrial organic solids) and steady in supply. Biogas produced from sewage sludge digestion is particularly useful because of its stable composition, containing a high fraction of methane and a low level of sulphur.

Electricity production on average sewage treatment plant sites (about 100 kW_{el}) is typically obtained from gas engines. However, depending on lifetime and operating conditions of the engine, electrical conversion is then relatively low (1) and may not suffice to cover the site's annual electricity needs, while heat production recovered from the engine can be in excess of the site requirements, i.e. space heating and maintaining the digesters temperature (35°C). In such a situation, the electricity deficit has to be bought in and the excess heat rejected. Fuel cells, owing to higher electrical efficiency, could thus better fit the plant needs with an output higher in electricity and lower in heat, from the on-site generated biogas.

Amongst fuel cells for biogas conversion, the high temperature solid oxide fuel cell type (SOFC) is especially suited, because of the capability of thermally integrated biogas reforming and because of manageable tolerance against fuel contaminants (1). A 1 kW_{el} SOFC unit (900°C) from Sulzer HEXIS, Switzerland, was succesfully operated (28 % LHV efficiency) on farm biogas in Switzerland for one year (2). Fuel Cell Technologies (FCT) from Canada demonstrate 5 kW_{el} SOFC units (46% LHV efficiency), also for biogas application (3). A tubular SOFC system of 100 kW_{el} (1000°C) has been tested, not with biogas, but with pipeline natural gas, for a succesful 2-year run (4) achieving 47% LHV electrical efficiency. Because of the similarities between natural gas and sewage biogas in fuel reforming and final sulphur levels, such a system can no doubt be operated also on the latter of the two fuels. The same argument applies to a planar SOFC system, shown recently to achieve 5.4 kW_{el} (38% efficiency) on steam-reformed methane (5). This unit operated at lower temperature (800°C) owing to the use of anode supported thin electrolyte cell (ASE) fabrication technology (20 x 20 cm cells, 361 cm^2 active area), that possess lower internal resistance loss. This technology (planar ASE) will be refered to in the system model study presented here.

A previous system model study, for a SOFC unit of a few kW_{el} converting farm biogas using partial oxidation as fuel processing step, was published by the present authors (6). Partial oxidation had been chosen as the most practical and economical solution for such a small system. Phenomena such as gas diffusion limitation and the risk of carbon deposition, left unquantified in the previously used model, were implemented in the presently improved model.

This study is concerned with a sewage treatment plant, producing roughly 100 kW_{el}-equivalent. At this size, steam reforming as fuel processing step is prefered to partial oxidation, for its higher efficiency and more appropriate thermal integration (endothermicity) with the fuel cell stack. Special attention to thermal management will be given here. The different fuel processing options will be compared.

Real data from an existing sewage sludge treatment plant, producing continuously ca. 1000 m^3 biogas per day, is taken as input to the SOFC system model. The aim is to demonstrate, using the solid oxide fuel cell instead of the gas engine, that site self-sufficiency in electricity and heat production from the generated biogas can be attained, resulting in depollution of its waste stream - which constitutes the primary purpose of the plant - at no net energy cost.

2. Experimental

Biogas samples from sewage sludge digestion plants (two different sites) have been periodically collected in glas bottles and analysed for their chemical composition, using a series of techniques. The levels of the main constituents were determined by gas chromatography (GC), using a Micro-gaschromatograph CP2300 from Varian Inc., Zug, Switzerland, equipped with a Poraplot-Q column and thermal conductivity detector. The averaged composition was used as input to the SOFC system model, together with site production data such as the hourly biogas flowrate.

Microcontaminant levels were determined by total combustion with O_2 followed by ion-exchange chromatography (for Cl, F, S), species-sensitive gas chromatography (for mercaptanes), mass

spectrometry (MS, for siloxanes and chlorofluoro-hydrocarbons) and MS combined with GC (for complex hydrocarbons). Details of these analyses are outside the scope of this paper and will be reported separately.

The model was defined via a graphical user interface in the programme "VALI" from the company BELSIM (Liège, Belgium). VALI is an equation-based data reconciliation software, including an extensive thermodynamic data base, used in petrochemical, chemical and power plants. Plant data are reconciled and computed in such a way that mass and heat balances are satisfied. The plant under study is implemented in a process flow diagramme, using streams (gas, liquid, or both) to connect equipment units (a reactor, a heat exchanger, a pump,...). The complete model constructed here contained a total of 192 variables and equations. Typical computing time of one run, i.e. the steady state output of the plant for a given set of input parameters, is on the order of seconds. Output is stored in tags and given as (i) the stream compositions at any position in the process flow scheme, as (ii) the heat consumption or generation of each equipment unit, as (iii) temperature inlets and outlets, etc. A graphical MATLAB interface, programmed in house, allows to scan the variation of a particular parameter (e.g. the CO_2 fraction in biogas, the biogas flowrate, the steam-to-carbon ratio, the excess air ratio λ used in the fuel cell stack,...) and record the output of every computational run. Finally, output is also represented as composite curves versus heat flux (kW).

3. Model

The process flow scheme implemented in the steady state model is depicted in Fig.1. Streams are numbered 1 through 8. Biogas composition, based on experimental data, is precisely defined in stream "1", which is preheated and mixed with preheated steam (which will be the reference case) and/or air for conversion to synthesis gas in the reformer. This is carried out at the same temperature as that of the fuel cell stack (800°C), assuming thermally fully integrated reforming. Cathode air is preheated to an inlet temperature of minimally 650°C (i.e. a maximum of 150 K below the stack temperature). Inlet air is 50% humid and contains a dry fraction of 79% nitrogen.

Inlet flows are circulated by blowers (1.1 bar, i.e. allowing for 100 mbar pressure drop in the various system units). At stack temperature, air flow is divided into a pure oxygen stream ("4a") deviated to the anode - this separation effectively representing the solid electrolyte - and the excess stream "4b", which combines with the anode outlet (stream "7") to completely convert the fuel residue to products in the afterburner zone, the adiabatic temperature of which is calculated. Transfered oxygen (stream "4a") and converted fuel (stream "6" minus stream "7") are connected and determined by a fixed value for the fuel utilisation u_f, typically set to 80%. All input streams are cold fluxes and require heat input (the Q-arrows in Fig.1). The exhaust is the only hot flux, from which heat is recovered to preheat all inputs. The stack represents a hot source (heat generation) and the reformer a cold source (heat absorption), both at constant temperature (800°C). Electrical power is removed from the stack, consisting of SOF cell plates 20x20cm large (361 cm^2 active area each) connected in series. The total heat balance represents the thermal efficiency of the system.

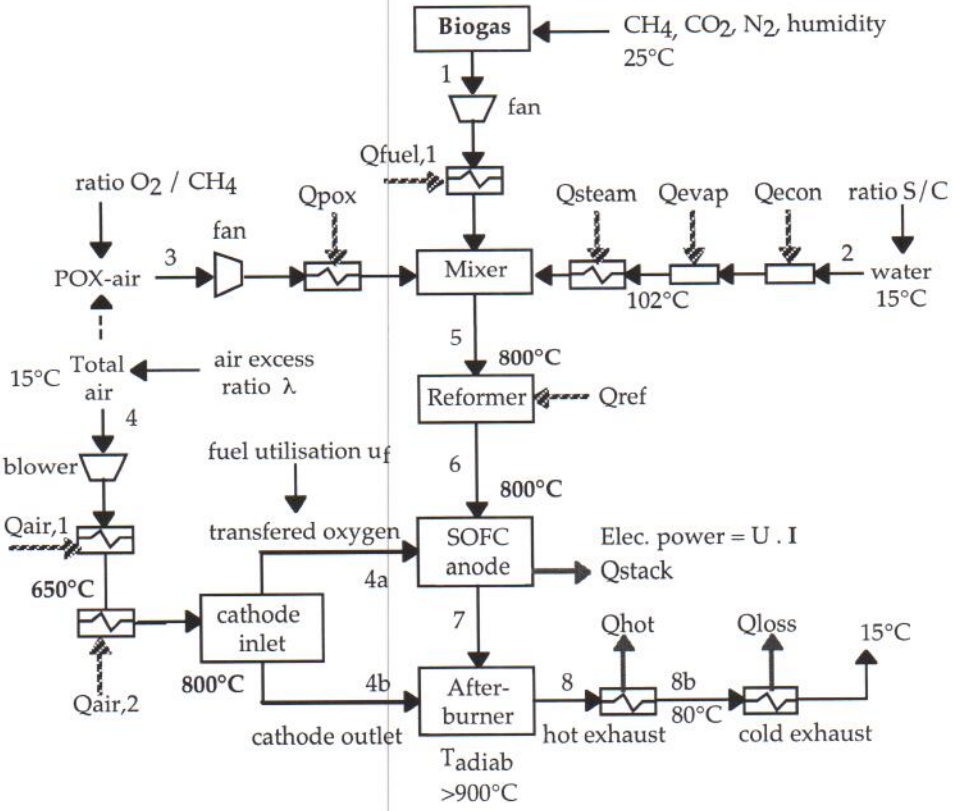

Fig. 1: Process flow diagramme of a Solid Oxide Fuel Cell system fed with sewage biogas

3.1. Electrochemistry

The electrochemical model for fuel conversion in the stack was elaborated in detail in a previous paper (6). Empirical expressions for cathode and anode activation polarisation loss were defined, as well as one for total ohmic losses (including metal interconnects and geometry effects). For the present study we added limitations for diffusion at anode and cathode. They have been taken into account, not by using diffusion coefficients applying to the given geometry (7), but by the basic expressions (8):

$$\eta_a = \frac{RT}{2F}\ln\left[1-\frac{j}{j_{lim}}\right] = \frac{RT}{2F}\ln\left(1-u_f\right) \qquad (1a)$$

and

$$\eta_c = \frac{RT}{2F}\ln\left[1-\frac{j}{j_{lim}}\right] = \frac{RT}{2F}\ln\left(1-\frac{u_f}{\lambda}\right) \qquad (1b)$$

for anode and cathode diffusion overpotential η_a and η_c, respectively, where j_{lim} is the theoretical current density for 100% fuel or oxygen conversion (λ denotes the cathode air excess). Whereas this description oversimplifies the diffusion process in fuel cell electrodes, it displays the merit of correctly "bending down" current-voltage response of the fuel cell at high fuel utilisation, as is observed experimentally. In particular expression (1a) for the anode likely overestimates the diffusion overpotential loss - but does bear reference to the fact that a thick support electrode of limited porosity is assumed to be used.

All voltage losses defined in the model are simultaneously plotted in Fig. 2 as a function of current density, where, in order to plot equations (1a) and (1b), which require knowledge of the limiting current (i.e. the fuel input flow), the latter is fixed for simplicity at 0.5 A/cm^2. An appropriate current density regime, where long term stability >40'000 h has been proven, is around 0.2-0.4 A/cm^2 (9, 10). High current density on smaller cells and stacks has of course been demonstrated, also for considerable operating time of 3000 h (11). Nonetheless, we decided to maintain the conservative estimates of Fig. 2, that are realistically obtained for SOFC systems today, and to not extrapolate

individual best data for general future projections. High current operation also increases heat generation on the stack, implying design constraints for cooling (high air flow, sufficient reforming endothermicity), as shown further on.

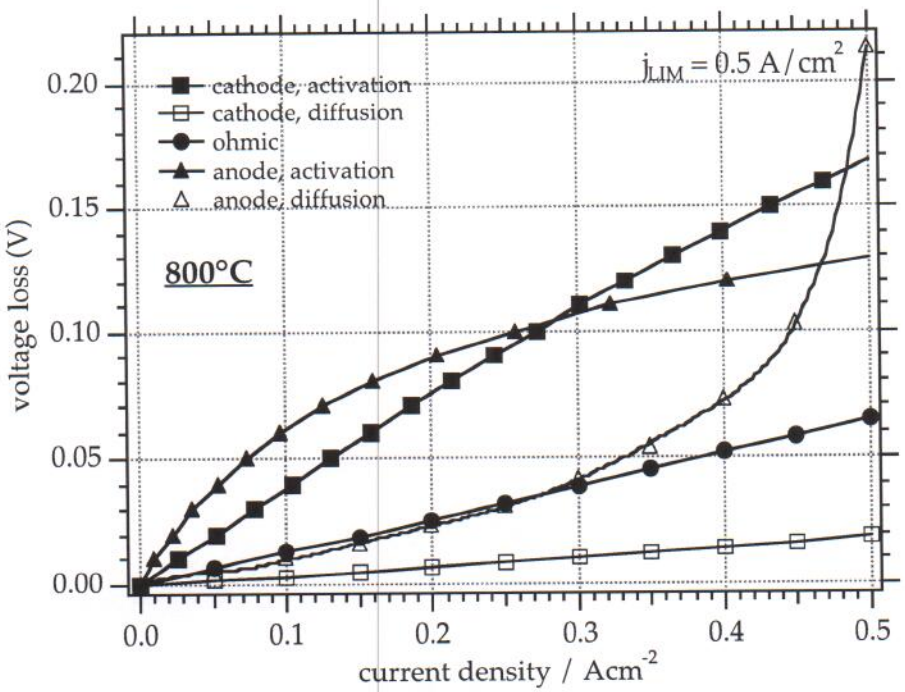

Fig. 2 : Voltage loss equations for anode and cathode used in the electrochemical model of the fuel cell stack, based upon ref.(6) and eq. (1). $R_{ohmic} = 0.13\ \Omega cm^2$. To illustrate the simple diffusion overvoltage loss (eq. 1), a limiting current of $0.5\ A/cm^2$ was taken as example (λ=3 for the airflow).

3.2. Carbon deposition

Likelihood of sooth formation from the fuel mixture is taken into account by considering the 3 reactions :

methane pyrolysis $CH_4 \Leftrightarrow C + 2H_2$ (2a),

Boudouard disproportionation $2CO \Leftrightarrow C + CO_2$ (2b),

and reverse gasification $CO + H_2 \Leftrightarrow C + H_2O$ (2c),

for which the equilibrium constants, K^{eq}, at given temperature and pressure are calculated from the thermodynamic properties of the reaction compounds. These K^{eq} are then compared against observed values, K^{kin}, calculated from the actual molar fractions (x_i) and total pressure (P_{tot}) for a given stream :

$$K^{kin}_{pyr} = \frac{p^2_{H_2}}{p_{CH_4}} \cdot \frac{1}{p^\circ} = \frac{x^2_{H_2}}{x_{CH_4}} \cdot \frac{P_{tot}}{p^\circ} \qquad (3a),$$

$$K^{kin}_{Boud} = \frac{p_{CO_2}}{p^2_{CO}} \cdot p^\circ = \frac{x_{CO_2}}{x^2_{CO}} \cdot \frac{p^\circ}{P_{tot}} \qquad (3b),$$

$$K^{kin}_{RevGas} = \frac{p_{H_2O}}{p_{H_2} p_{CO}} \cdot p^\circ = \frac{x_{H_2O}}{x_{H_2} x_{CO}} \cdot \frac{p^\circ}{P_{tot}} \qquad (3c).$$

In a third operation, after logarithmisation, observed values are then compared against the theoretical ones. The result of the operation

$$\ln\left[\frac{K^{kin}}{K^{eq}}\right]$$

then indicates whether carbon deposition occurs (result ≤ 0) or not (result > 0), for each of the 3 equations. This calculation was performed for stream "6" in the model. Care was taken to always observe sufficiently positive values for the 3 operations, whenever changing inlet fuel composition.

Fig. 3 plots the equilibrium values, K^{eq}, versus temperature for the 3 reactions (2a)-(2c). It clearly illustrates the critical temperature range from ≈560°C to ≈660°C, where the tendency for carbon formation is positive for all 3 reactions simultaneously (or in other words, the standard free enthalpy of all 3 reactions is negative in this temperature range).

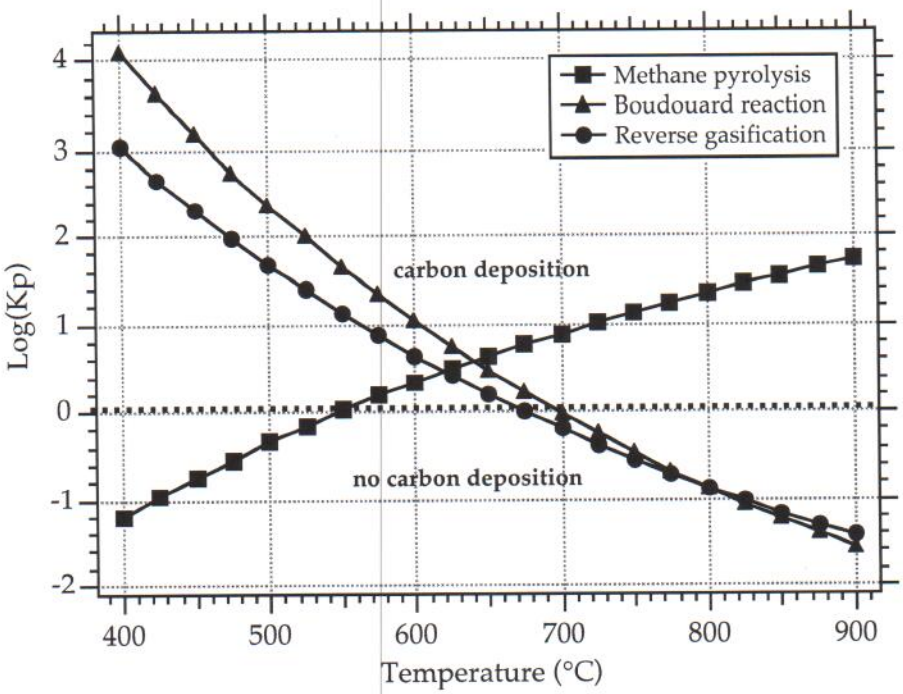

Fig. 3 : Equilibrium constants, K_p, for the three considered carbon formation reactions (eq. 2), as a function of temperature.

4. Results and discussion

4.1. Biogas composition and production

The level of the main constituents CH_4, CO_2, O_2, N_2, H_2O (vol%) as well as of H_2S (ppmv), of digestion gas from two local sewage treatment plants was measured regularly during several months. Oxygen and nitrogen were not separated on the GC column and are therefore taken as a sum-value ("air-peak"). Water vapour content was not measured but taken as the difference between 100% and the sum of the signals for CH_4, CO_2 and air, these latter three having been precisely calibrated on known premixed gases. Table 1 summarizes the data. All entries represent averages of minimum 20 consecutive measurements on the same sample (total analysis time ≈ 3 h).

Table 1 : Measured biogas compositions of 2 sewage plants (≈100 kW_e) over the period Jul-Nov 2002

Site 1	$\%CH_4$	$\%CO_2$	$\%(N_2+O_2)$	$\%H_2O$	ppm H_2S
	63.33	33.74	1.14	1.79	1.52
	63.59	33.13	0.28	3.00	0.40
	62.16	35.48	0.87	1.49	1.21
	63.03	33.85	1.07	2.05	2.28
	63.55	34.25	0.75	1.45	3.77
	61.60	36.37	0.92	1.11	2.28
	63.28	34.39	1.30	1.03	2.42
	60.75	36.79	0.87	1.59	1.44
	64.42	34.52	1.06	dry	-
	60.52	35.78	0.92	2.78	-
Mean	62.62	34.83	0.92	1.81	1.92
Site 2	60.10	37.43	0.21	2.26	0.66
	64.05	35.08	0.12	0.75	0.75
	62.47	36.21	0.10	1.22	2.15
	65.22	32.10	0.15	2.53	0.53
	63.67	35.75	0.57	dry	-
	62.81	35.78	0.39	1.02	-
Mean	63.05	35.39	0.26	1.56	1.02

From Table 1, we derive and define an average sewage biogas composition of 63% CH_4, 35% CO_2, 0.5% air and 1.5% H_2O. H_2S, which is noted at a very low concentration of 1-2 ppm, is not further taken into consideration. This biogas would not require sulphur cleanup (e.g. by active carbon filters or ZnO reactors) before admission to the SOFC reformer and anode catalysts.

Actual yearly production data for "Site 1" (Table 1) are given in Table 2. Values have been averaged for six consecutive years (1997 through 2002).

Table 2 Production data of an existing sewage treatment plant averaged over the period 1997-2002

BIOGAS		
Biogas production	m^3/yr	378439.5
Used in the 130 kW engine	%	87.7
Used in a boiler	%	2.9
Flared off	%	9.3
Equivalent biogas per inhab.	L/day	36.1
Methane equivalent in engine (63%)	m^3/d	571.8
ELECTRICITY		
Yearly engine hours	h/yr	5613.3
Average daily engine hours	h/day	15.4
Electricity production	MWh_{el}/yr	463.0
Average load	kW_{el}	82.7
Methane input in engine, HHV (J)	MWh/yr	2187.0
Methane input in engine, HHV (W)	kW_{el}	391.5
Efficiency HHV	%	21.2
Site consumption	MWh_{el}/yr	913.2
Site self-sufficiency	%	51.9
WASTE WATER		
Waste water entry (WW)	m^3/yr	4'591'667
Fresh sludge	m^3/yr	22107
Decanted sludge to digester	m^3/yr	11151
Digested sludge out	m^3/yr	1965
Biogas per organic dry matter (ODM)	m^3/t	633.7
Organic charge in sludge	%	5.5
$FeCl_3$ consumption (42%-solution)	t/yr	284.7
Fe equivalent	g/m^3WW	8.6

Yearly biogas production is an average 378'440 m^3 (1036 m^3/day), of which ≈88% is consumed by the gas engine, operating for about ≈15 h/day. This leads to an electricity production of 463 MWh/yr, only 52% of the site requirement (913 MWh/yr). Note the low average efficiency of the 130 kW engine (21%). The equivalent biogas production per inhabitant, connected to this sewage network, amounts to 36 L/day. At 63% of methane content, this figure (8.3 m^3 CH_4/yr), extrapolated to the actual European Community (EU-15, 375 mio inhabitants), leads for this region to an ultimate potential of 2.67 Mtoe (million tonnes oil equivalent), corresponding to an installed electricity generation potential of over 1 GW (≈10'000 sites of ≈100 kW_e). Estimates for the actually exploited sewage biogas in Europe range from 0.34 to 0.58 Mtoe (12,13).

From the biogas production in Table 2, an hourly rate of 43 m^3 is derived, which is used in the SOFC system model as input value. It corresponds to an higher heating value (HHV) input of 269 kW (lower heating value or LHV of 242 kW).

No data on the heat requirement or consumption are measured on site. Heat is recovered from the engine cooling water and hot exhaust fumes, to provide space heating and to keep the digester at optimal temperature (35°C). This suffices to cover annual thermal needs, with a large surplus in summer (rejected) and only a very slight deficit in winter, during which a total of around 1000 m^3 of natural gas (i.e. corresponding to < 2 days of biogas production) is burned in the boiler for supplemental heating.

Note finally the important consumption in iron chloride solution, added to the incoming waste water for cold desulphurisation, and leading to the low sulphur content in the biogas product.

4.2. Determination of model input parameters

Reforming conditions

Steam has to be added to biogas (in this case the methane-carbon dioxide mixture in proportion of 63:35) in order to avoid carbon formation. The minimum steam quantity required, at a given temperature, can be determined from thermodynamic equilibrium concentration calculation, and is plotted in Fig. 4 as the steam-to-carbon ratio (S/C, mole H_2O vs. mole C) in the inlet mixture. At 800°C, the minimal S/C value is determined to 0.37. To introduce a safety factor, S/C is chosen to 0.5 for the subsequent model calculations, effectively corresponding to a ΔT of -70 K. This means that, in practice, the endothermal reformer could be allowed to cool from 800°C to 730°C (during transients, or because of inertia), without running into thermodynamic risk of carbon deposition. Fig. 4 shows that for S/C = 1.3, carbon formation is theoretically excluded at any temperature.

Also displayed in the graph is an equivalent condition when using partial oxidation as fuel processing step (6). The minimal oxygen-to-methane ratio necessary to avoid sooth building from the 63:35 CH_4:CO_2 mixture at 800°C is 0.27. As partial oxidation is fast and exothermic, and as we

cannot allow the O_2/CH_4-ratio to reach high values (to keep the electrical efficiency at a respectable level), O_2/CH_4 is limited to 0.3. This choice, corresponding to a ΔT of -20 K, will also be applied as syngas formation condition for the SOFC system model (see §4.5), to compare with steam-reforming.

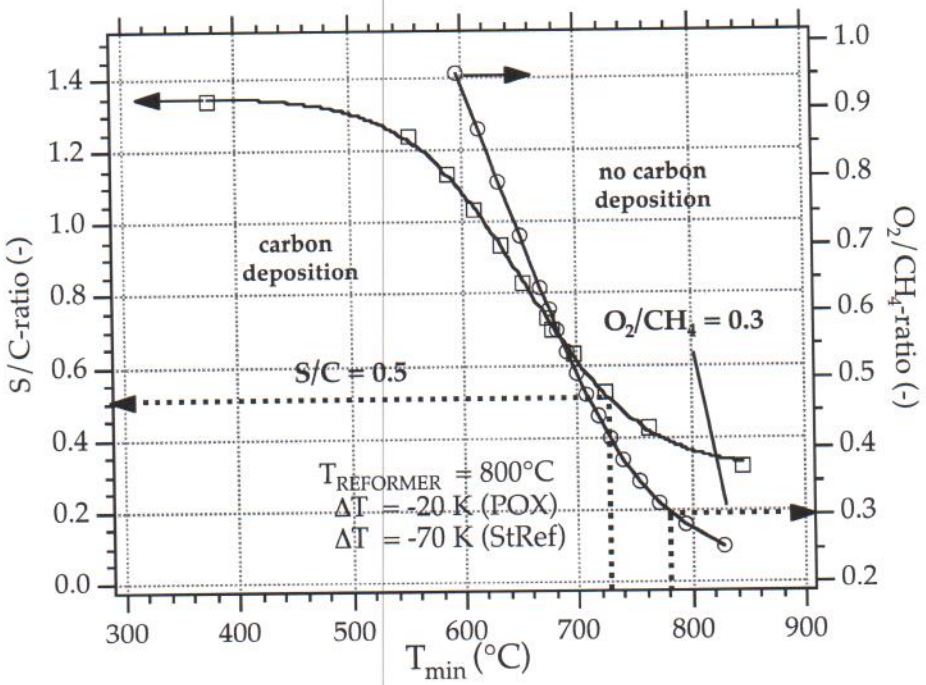

Fig. 4: Minimal temperature and corresponding required ratios of steam-to-carbon (S/C) and oxygen-to-methane (O_2/CH_4) above which no carbon deposition takes place thermodynamically.

Reference case

Using the condition S/C = 0.5 at the fuel inlet - in the following denominated as "reference case" - thermodynamic equilibrium concentrations as a function of temperature (such as those corresponding to the reformer outlet stream, at 800°C) are given in Fig. 5. The input fuel is now defined by the generic formula $C_{0.98}H_{3.52}O_{1.2}N_{0.004}S_0$. At each temperature in the graph this atomic balance can be verified. At the reforming temperature of 800°C, conversion to syngas is fairly complete and the H_2/CO ratio around 1.8, in between that of pure steam-reforming (H_2/CO = 3) and that of dry

reforming (H_2/CO =1) since we effectively deal with mixed reforming of CH_4 with both H_2O and CO_2. This is simply derived from the nominal reactions, with S/C = 0.5 and a CO_2 fraction of 35%:

$$\begin{aligned} 0.5 * \quad & (CH_4 + H_2O \Leftrightarrow 3H_2 + CO) \\ 0.35 * \quad & (CH_4 + CO_2 \Leftrightarrow 2H_2 + 2CO) \end{aligned} \tag{4a}$$

adding up to :

$$0.85\,CH_4 + 0.5\,H_2O + 0.35\,CO_2 \Leftrightarrow 2.2\,H_2 + 1.2\,CO \tag{4b}$$

and normalising to the input of 0.63 mole methane per mole of biogas :

$$0.63\,CH_4 + 0.37\,H_2O + 0.26\,CO_2 \Leftrightarrow 1.63\,H_2 + 0.89\,CO \tag{4c}$$

The last equation proves the H_2/CO-ratio of 1.63/0.89 = 1.83 (Fig. 5) and also that 0.12 mole of initial steam and 0.09 mole of initial carbon dioxide remain unreacted, as evident in the figure. Concentration variations in H_2, H_2O, CO and CO_2 above 800°C (with vanishing CH_4 and absence of carbon) are then only governed by the shift reaction.

The dotted line indicates the open circuit voltage (OCV) that would be observed for a perfectly sealed cell with the anode inlet gas composition defined in Fig. 5 at each corresponding temperature with respect to air (pO_2 = 0.21 atm) at the cathode. OCV at 800°C is then 1.05 V.

The stoichiometric oxygen amount needed to burn all fuel is given by :

$$\frac{n_{O_2}}{n_F} = n_C + {}^{n_H}\!/_4 - {}^{n_O}\!/_2 = 0.98 + 0.88 - 0.6 = 1.26 \quad (u_F = 100\%) \tag{5}$$

obviously leading to 2 mol-equivalent of oxygen per mole of methane (2*0.63=1.26) as essentially no free oxygen is present in the fuel (0.1%, which is neglected).

Adding oxygen to the reformed fuel (stream "4a" to stream "6"), anodic oxidation proceeds and the outlet composition is calculated as a function of fuel utilisation, u_F, plotted in Fig. 6, showing the consumption of H_2 and CO fuels and formation of H_2O and CO_2 products. Also shown is the

corresponding OCV, dropping to 0.87 V at the outlet for 80% fuel utilisation. As the model computes the stack electrical output using the electrochemical losses defined in Fig. 2, that are subtracted from the free enthalpy of the reaction, in itself determined by anode plus cathode outlets minus inputs (OCV at the inlet 1.05 V, at the outlet 0.87 V), an average OCV value is to be considered, i.e. 0.96 V.

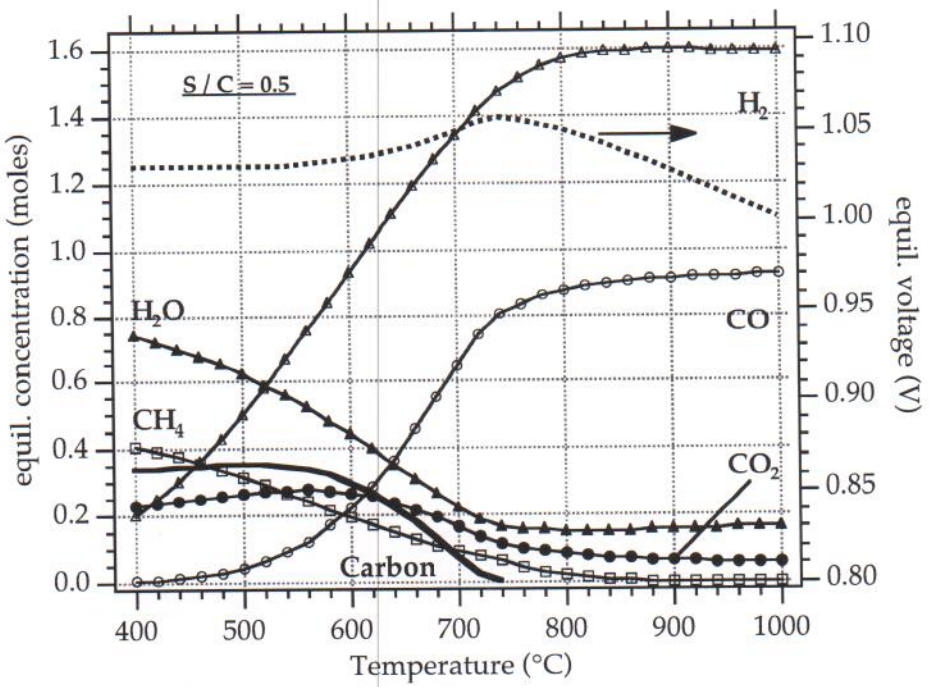

Fig. 5 : Thermodynamic equilibrium concentrations, as a function of temperature, for the fuel mixture consisting of 1 mole biogas (63% CH_4, 35% CO_2, 1.5% H_2O, 0.5 % N_2) with 0.475 mole water, corresponding to a S/C ratio of 0.5. Molar concentrations normalised to 0.98 moles of carbon in the mixture.

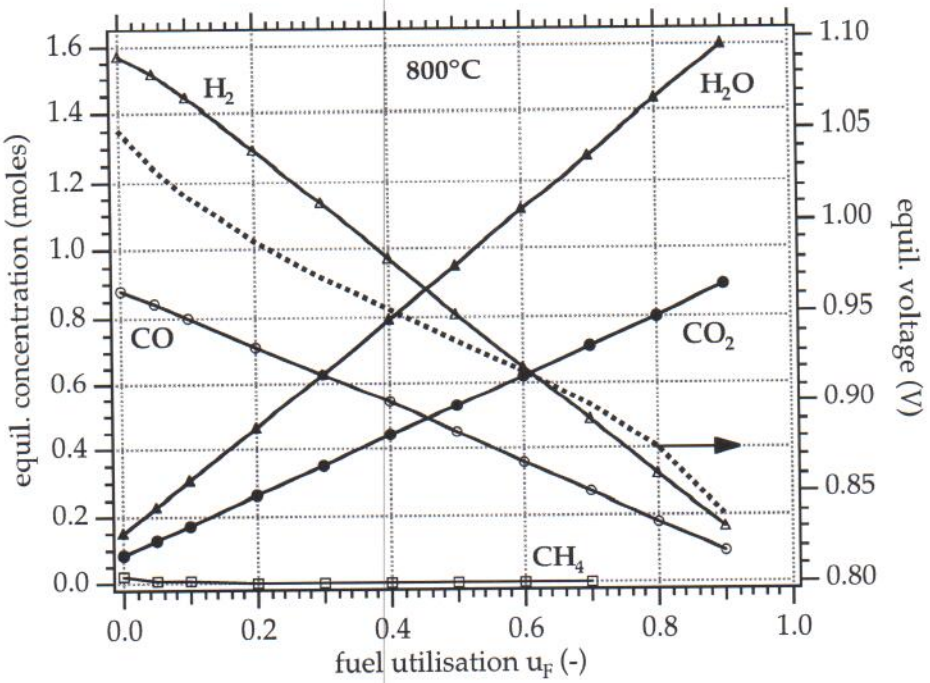

Fig. 6 : Thermodynamic equilibrium concentrations, as a function of fuel conversion (%), i.e. as a function of 0-90% oxygen addition, for the product mixture of 1 mole biogas (63% CH_4, 35% CO_2, 1.5% H_2O, 0.5 % N_2) and 0.475 mole water at 800°C (see Fig. 5). Molar concentrations normalised to 0.98 moles of carbon.

Air excess ratio

A multiple quantity of the stoichiometric oxygen amount, indicated by the factor λ, is flown at the cathode for stack cooling. The overall fuel conversion reaction is therefore written :

$$\begin{aligned} & C_{0.98}H_{3.52}O_{1.2}N_{0.005} + 1.26 * \lambda * (O_2 + 3.773\, N_2) \\ & \Rightarrow 0.98\, CO_2 + 1.76\, H_2O + 4.754\, N_2 + 1.26 * (\lambda - 1)\, O_2 \end{aligned} \qquad (6)$$

When λ=1, the water vapour fraction in the outlet is maximal and equal to 23.5%. With an empirical formula for the saturation pressure :

$$P_{sat}(Pa) = \exp\left[23.57 - \frac{4041.6}{T_{sat}(°C) + 235.6}\right] \qquad (7)$$

we obtain 64°C for the temperature at which water vapour will start to condense from the mixture. Usually λ is higher, so T_{sat} will be lower still. Nevertheless, outlet temperature for the cold exhaust fumes (Fig. 1, stream "8b") was fixed to a realistic 80°C, without recovering condensation heat.

Given the biogas inlet flow (43 m^3/h), the fuel utilisation (0.8) and the electrochemical losses (Fig. 2), the necessary number of cells for the stack can be estimated. Before, two further assumptions are made. First, λ is for the moment postulated at the factor 3, a common value for steam-reformed methane driven stacks (14). Second, a minimal cell operating voltage of 0.65 V is postulated. We indeed observe experimentally that cell degradation accelerates below such operating voltage, which can be related to the reduction-oxidation potential of the nickel anode catalyst (15).

Following the previous arguments, a cell loss of around 310 mV can therefore be tolerated (0.96 V OCV - 0.65 V operating voltage). Combined diffusion losses, from eq. (2) with u_f=0.8 and λ=3, can be determined to 89 mV. Hence, activation and ohmic loss can total approximatively 220 mV. From Fig. 2, we then obtain a corresponding current density of 0.24 A/cm^2, or 86.4 A on the stack (361 cm^2 active area per cell).

43 m^3/h of biogas (63% methane) correspond to an input flow of 0.5 mole CH_4/sec. Stoichiometric oxygen implies 1.26 times this flow, but u_f is fixed to 0.8. Therefore, the oxygen flow through the electrolyte membrane (stream "4a") is 0.51 mole/sec. Converting to current (*4*F), this equals 196560 A for one hypothetical cell. With the stack current determined to 86.4 A, the ratio of both values gives the required cell number, i.e. ≈2400.

This value is very large and due to the purposefully chosen conservative loss characteristics (Fig. 2), equivalent to an area specific resistance (asr) of around 1.2 Ωcm^2. Our own ASE cells presently show an asr of ca. 0.6 Ωcm^2 (16), so that half the amount of cells (i.e. 1200) could eventually suffice to construct the 100 kW_e sized stack, with a obvious enormous impact on cost. For comparison, the demonstrated 100 kW_e tubular SOFC stack (4) used 1152 tubes of ≈1000 cm^2 active area each.

Excess air λ had been postulated to the factor 3 above. In the following, justification for this choice is given through consideration of the stack thermal balance . Heat developed on the stack (Q_{stack}) because of the exothermal reactions has to be evacuated to avoid thermal runaway. This can be accomplished by the endothermal reformer, in thermal conctact with the stack, on the one hand, and on the other hand by the gases transiting the stack, especially the cathode air excess flow. Fig. 7 gives the evacuated heat (in kW) for the reference case considered (43 m^3/h biogas input flow with S/C=0.5). In particular, heat flux required to heat anode and cathode (depending on λ) gases over a certain temperature difference ΔT are plotted. It appears, once the fuel input flow and the reforming mixture are fixed, that the air excess and the allowable ΔT are the only control variables that can regulate heat removal from the stack, the small anode gas flow playing a minor role. A maximum ΔT of 200 K is admissible (17, 18). This may be brought in relation to thermal stress of the ceramic materials that compose the stack. Stress accumulation in a material due to a thermal gradient may in a simple form be expressed as (19):

$$\sigma\,(\mathrm{MPa}) \;=\; \alpha.\Delta T.E_Y \qquad (8)$$

with α the thermal expansion coefficient in m/m.K and E_Y the materials Young modulus in Pa. Using order of magnitude values of $\alpha = 10^{-5}\ K^{-1}$ and $E_Y = 10^{11}$ Pa for the ceramics, a ΔT of 200 K leads to thermal stress of 200 MPa, close to the modulus of rupture of for example the electrolyte material at high temperature (20). Similarly, an tolerable diagonal gradient on the proposed planar ASE cells has been reported to 0.7 K/mm (21), hence ca. 200 K on a 20 x 20 cm square cell. For this reason, air at the cathode inlet in the system model may be as low as 650°C as minimal temperature, and the outlet (streams "4b" and "7") up to 850°C at most, in order to limit materials deterioration. Especially the cheap metal interconnects used for cell stacking (FeCr alloys) cannot tolerate temperatures above 850°C in an atmosphere with high steam levels for a long time (22).

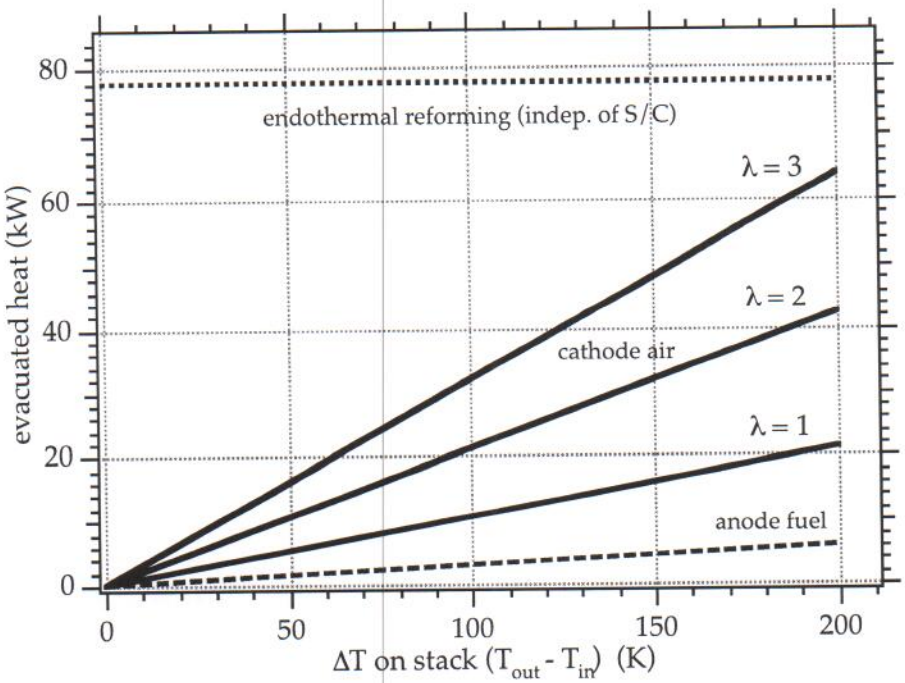

Fig. 7 : Heat sinks (in kW) provided by endothermal reforming and circulating gases, as a function of the air flow (λ) and of the thermal gradient on the stack (ΔT), to evacuate the heat generated in the fuel cell stack.

Fig. 8 displays the balance between heat generation on and cooling of the SOFC stack. For the chosen input conditions (discussed higher and summarised further in Table 3), electrical and thermal power developed on the stack are 131 kW_{el} and 143 kW_{th}, depending somewhat on the circulating air excess. The curve denoted "stack cooling power" adds up the evacuated heat fluxes (Fig, 7) by the reformer (78 kW) and the cathode air for a ΔT equal to 200 K ($Q_{air}= \lambda^*21$ kW). Stack heating and cooling are exactly balanced at λ=3.

The preceding argument of course is a rather artificial construction. In physical reality, the stack may experience further heating from an afterburner zone in proximity and cooling because of insulation losses. However, the simple representation used here illustrates the general argument of fuel cell stack thermal balancing by easily tracable numbers in a simplified system component configuration.

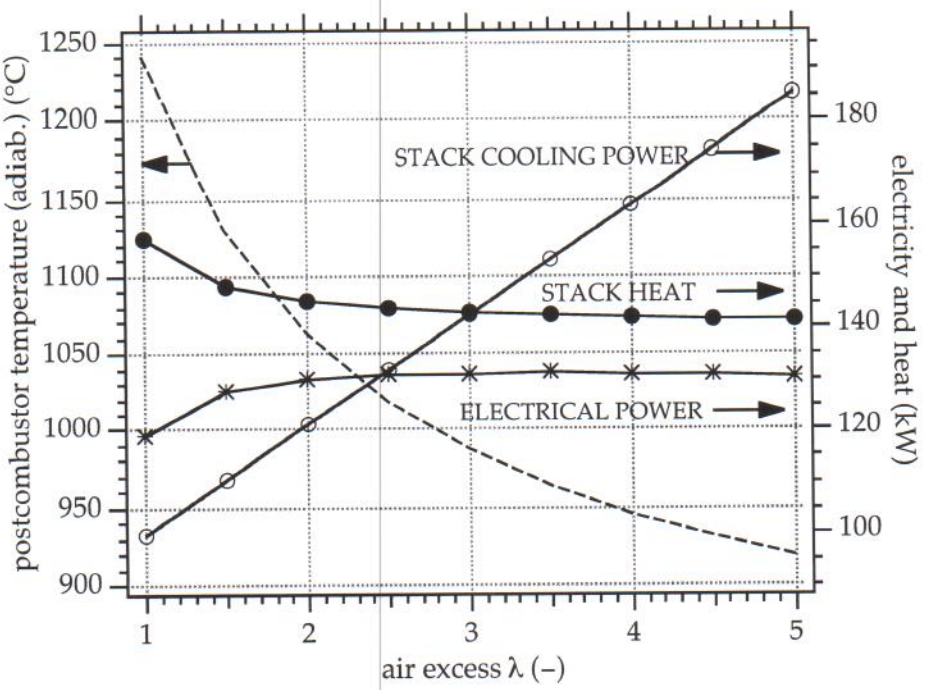

Fig. 8 : Generated electrical power and heat (kW) by the fuel cell stack, as a function of air flow (λ). Also shown as a function of λ is the cooling power (sum-curve from Fig. 7, with $\Delta T = 200$ K), as well as the hypothetical adiabatic temperature in the postcombustion zone. The reference case of steam reformed biogas (S/C = 0.5) is taken, $T_{stack} = T_{reformer} = 800°C$.

4.3. Model output : steam reformed biogas

Having in the previous sections defined, and motivated the selection of, all input parameters, the steady state model output for the reference case (steam reformed biogas, S/C=0.5) is discussed in the following. Table 3 lists all relevant resulting numbers, and Table 4 gives the stream compositions at different positions in the process flow scheme, whereas Fig. 9 plots the stack current-voltage behaviour at design fuel input (43 m^3/h).

Table 3 shows that 134 kW_e are obtained from the stack, leading after subtraction of 3 kW required to circulate the gases (850 m^3/h at 1.1 bar inlet) a net dc generation of 131 kW_e, at a HHV efficiency of 48.7%. The gas engine installed on site is precisely of 130 kW_e size. Generated heat in the stack is 143 kW_{th}, balanced by the reformer and the cathode air as discussed (Fig. 8). Available heat from the exhaust, when cooling from the afterburner outlet, 986°C, to the released fumes at 80°C, is 318

kW_{th}, sufficient to preheat air (187 kW_{th}) to stack inlet temperature (650°C), fuel (22 kW_{th}) and steam from reforming water (19 kW_{th}). The total heat balance amounts to +106 kW_{th} or almost 40% thermal efficiency (269 kW methane input).

Table 3: Input and output data of the process flow model for the reference case of steam reformed biogas (S/C = 0.5)

biogas inlet flow	43	Nm^3/h
methane inlet flow	27.1	Nm^3/h
fuel input power	269.3	kW
stack inlet temperature, air	650	°C
reformer temperature	800	°C
stack temperature	800	°C
cell area	361	cm^2
cell number	2400	-
air excess λ	3	-
steam-to-carbon ratio S/C	0.5	-
stack voltage	1553.9	V
cell voltage	0.648	V
current	86.37	A
current density	0.2393	A/cm^2
$\eta_{anode,act}$	0.0965	V
$\eta_{anode,diff}$	0.0744	V
$\eta_{cathode,act}$	0.0884	V
$\eta_{cathode,diff}$	0.0143	V
gross electric power	134.21	kW_{el}
air compressor power	-2.986	kW_{el}
fuel compressor power	-0.170	kW_{el}
net electric power	131.06	kW_{el}
gross elec. efficiency	49.83	%
net elec. efficiency	48.66	%
thermal efficiency	39.57	%
stack generated heat	142.95	kW
reformer cooling power	-78.24	kW
stack cooling air (ΔT 150 K)	-48.05	kW
hot exhaust	317.96	kW
main air preheater	-187.24	kW
fuel preheater	-21.72	kW
economizer	-1.70	kW
evaporator	-10.49	kW
steam preheater	-6.88	kW
cold exhaust loss	20.45	kW

Table 4 shows the reformer outlet is 90% syngas at nearly double the fuel inlet flow (116 m^3/h vs. 64 m^3/h), of which 80% is converted, or 116 *0.9*0.8 = 86.6 m^3/h, requiring just half of this in oxygen flow through the electrolyte membrane (stream "4a", 43.3. m^3/h). This stream, 12 L O_2/s through 2400 cells * 0.0361 m^2 = 87 m^2 of active area, of course translates to 0.24 A/cm^2 current density.

Table 4 : Stream compositions at various positions in the process flow, for the reference case of steam reformed biogas (S/C = 0.5), given in total flow (Nm^3/h) and in mole% per stream.

Mole%	Cathode	%	%	%	FUEL	%	%	%	%	%	%
Position	FLOW	O_2	N_2	H_2O	FLOW	CH_4	CO_2	H_2O	N_2	H_2	CO
Inlet	*780.5*	21	78.1	0.9	*63.9*	42.7	23.7	33.2	0.4	-	-
Reformer outlet					*116.2*	0.78	3.24	5.7	0.2	57.9	32.2
O_2 transfer	*43.3*	100									
Stack outlet	*737.2*	16.2	83	0.9	*118*	0	29.2	52.2	0.2	11.9	6.5
Postcomb. outlet	*844*	12.8	72.4				5	9.8			
Flow units	m^3/h				m^3/h						

Fig. 9 compares the conservative i-V output from the model with that of recent results obtained in house on anode supported electrolyte cells, from an 8-cell stack test of 50 cm^2 active area each, delivering 140 W_e below 800°C (0.32 W/cm^2) from H_2 fuel, however for lower fuel conversion (50%). The comparison illustrates the realistic performance estimate for the model stack. Efficiency reaches 49% and is maximal at 85% fuel utilisation, after which anode diffusion loss causes the operating voltage to drop steeply.

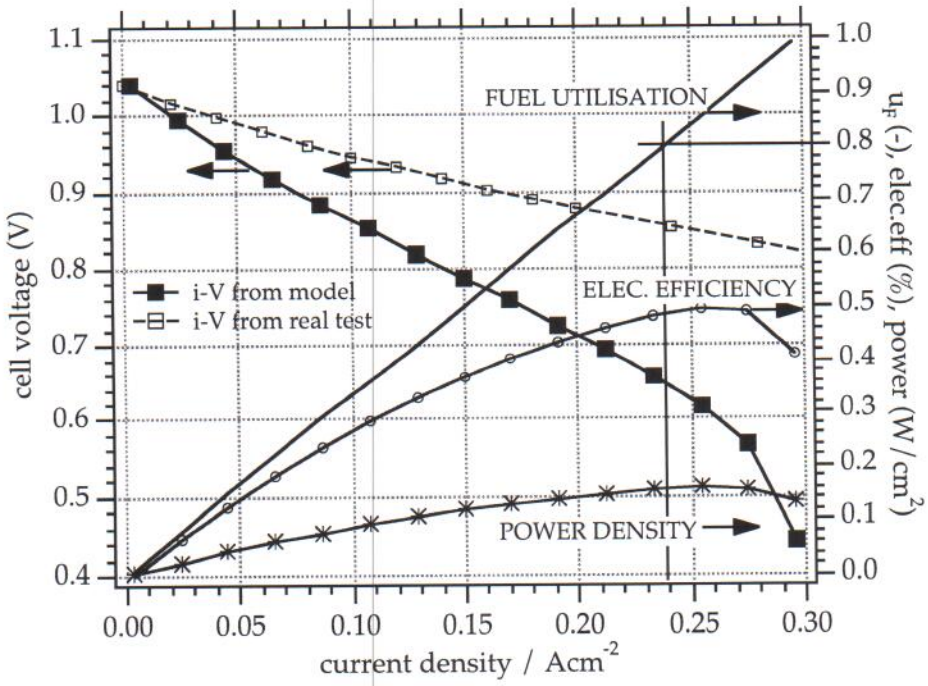

Fig. 9 : Current density - cell voltage- power density output for the model cell-stack (800°C), considering the reference case of biogas feed with S/C = 0.5. Electrical efficiency is seen to raise to 49%, at 80% fuel utilisation and 0.15 W/cm^2 power density. Also shown is the experimental cell output of an in-house developed stack (140 W_{el}, 800°C, u_F 50%), illustrating adequate realistic potential.

From another point of view, input methane of 269 kW is upgraded to 357 kW in the reforming process (78 kW input), of which 80% (i.e. 274 kW) is converted on the stack, namely 38% to electricity (131 kW) and 42% to heat (143 kW).

Fig. 9 is replotted in Fig. 10, converting current density to fuel utilisation, but focussing now on the thermal balance of the system, indicated in kW. Electrical power and exploitable excess heat ("thermal power") always add up to 238 kW (88.5% cogeneration efficiency), with the electricity fraction dominating the heat fraction once above 65% fuel utilisation. While electricity production flattens out (126 to 132 kW_e) between 70 to 90% fuel conversion, heat generation in this regime sharply increases (115 to 180 kW), requiring an adaptation in cathode air flow if materials exposure to excessive local temperature is to be avoided. Heat evacuation by reforming and cathode air (λ=3, ΔT=200K), totalling 142 kW, is also displayed.

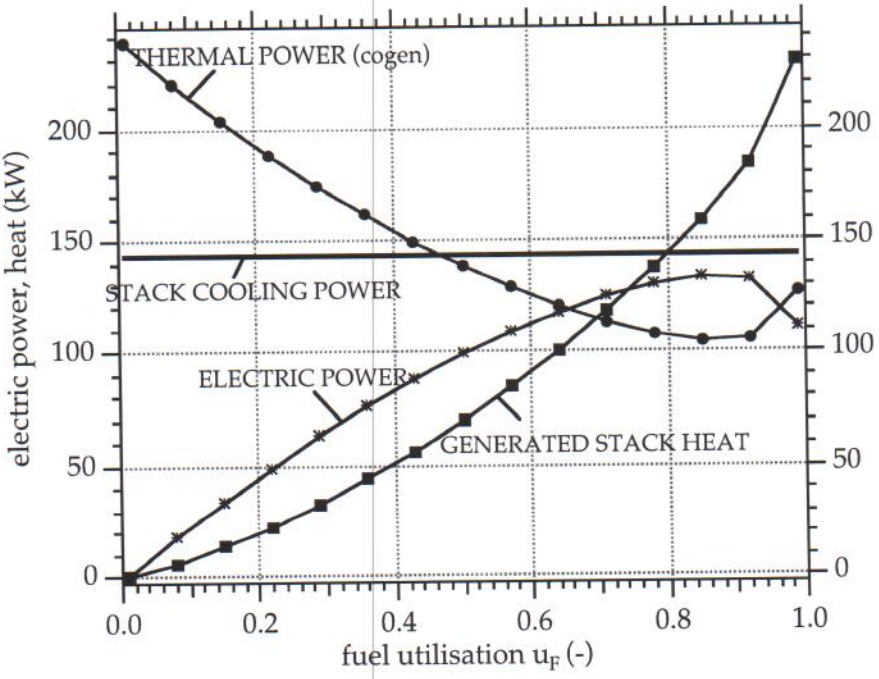

Fig. 10 : Heat balance of the fuel cell stack, as a function of fuel conversion. Generated electrical power and useful thermal output power balance out to a constant total output of ca. 238 kW (88.5% HHV cogeneration efficiency), but generated stack heat strongly increases at high fuel conversion, requiring appropriate cooling (by endothermal reforming and cathode excess air, here λ = 3).

4.3. Composite curves

The following three graphs Fig. 11 through 13 plot the composite curves for the reference case (S/C=0.5) of the biogas-SOFC system model.

In Fig. 11, the upper curve or hot composite is the sum of all hot fluxes and sources in the system, sorted by temperature-level : $Q_{exhaust}$ from the postcombustion temperature (986°C or 1259 K) down to 800°C, Q_{stack} as source at 800°C, and $Q_{exhaust}$ again from 800°C down to the final temperature (15°C) of rejection to the environment (which includes "Q_{loss}" from 80°C to 15°C, see Fig. 1). The bottom part of the hot composite fixes the scale of exchanged heat (x-axis, Q in kW) at zero. In total, 481.5 kW is available, as verified from Table 3 (Q_{stack} = 143 kW, $Q_{exhaust}$ = 318 kW, Q_{loss} = 20.5 kW). From the upper part of the hot composite (1259 K, 481.5 kW), the heat requirements of the system are satisfied "going backwards", i.e. the cold composite or the sum of all cold fluxes and utilities in the system (lower curve in Fig. 11) is traced back towards the left on the x-axis. These are : $Q_{reformer}$ (78 kW) as cooling utility (at 800°C, but shown displaced in the figure, at a level of 790°C, for clarity), preheating of air, steam and fuel between 100° and 800°C, evaporation of water to reforming steam (10.5 kW), and preheating of all fluxes between inlet temperature (15 or 25°C) and 100°C. The needs, as verified from Table 3 (i.e. all negative heat fluxes Q), total 355 kW. The difference between both hot and cold composite streams equals 126.5 kW, visible on the x-axis between origin and low temperature end-point of the cold stream. Subtracting the final loss to the environment (20.5 kW), the available cogeneration heat flux (106 kW, thermal efficiency 39.7%) is obtained. This heat is available at a temperature-level at least of the hot composite flux, at which all cold flux preheating is satisfied, i.e. 650 K in the figure.

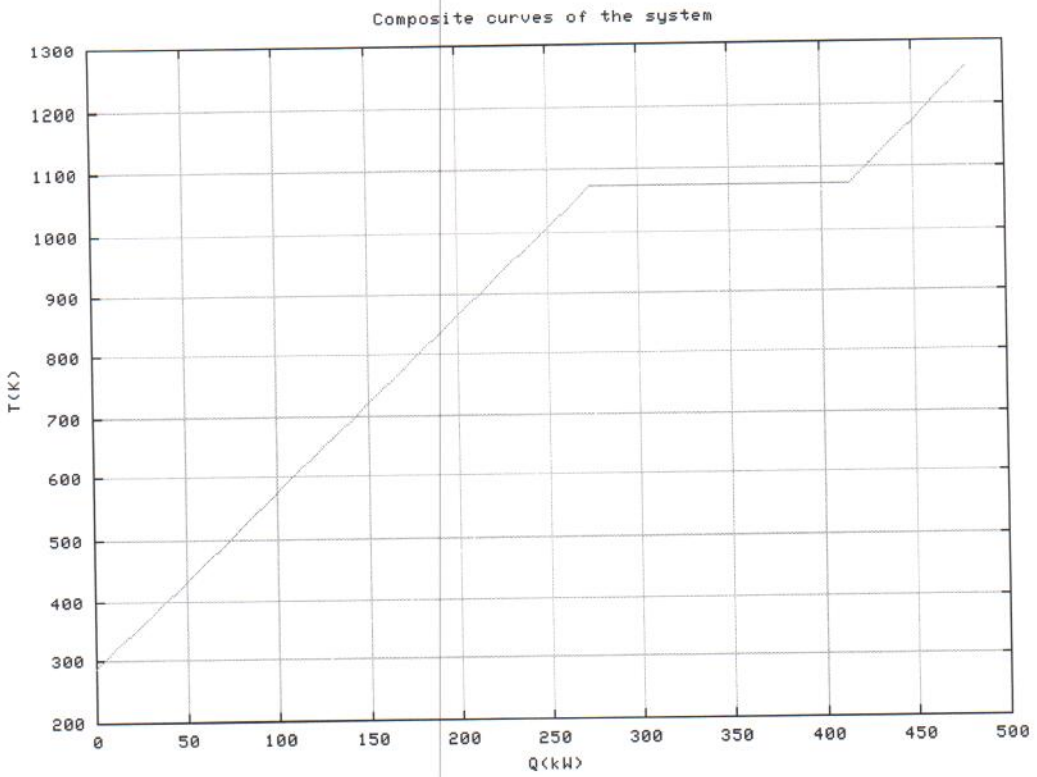

Fig. 11 : Hot and cold composite curves of the SOFC biogas system (S/C=0.5). Plateaus of stack heat generation, endothermal reforming and steam generation are easily recognized. Available excess heat (final difference between the 2 curves) is 126 kW.

Fig. 12 shows the grand composite curve of the system vs. heating power (kW), i.e. the difference between hot and cold composite fluxes (Fig. 11) or net heat flux between each 2 corresponding temperature levels. The origin of the x-axis is now placed at the highest temperature level (1259 K), starting with the hot exhaust from the afterburner, and plotting net heat generation towards the right and net heat absorption towards the left. Again the 3 isothermal plateaus corresponding to Q_{stack} (generation of 143 kW, at 800°C), $Q_{reformer}$ (absorption of 78 kW, drawn at 790°C, for clarity) and $Q_{evaporator}$ (absorption of 10 kW, at 100°C) are found. The grand composite shows that the available net heat flux of 126 kW (cogeneration heat), is actually available at the temperature of 800°C, i.e. at very high exergy value. Therefore, in reality, the overall electrical efficiency of the system could still be enhanced by pressurising the flows and adding an expansion microturbine to the exhaust.

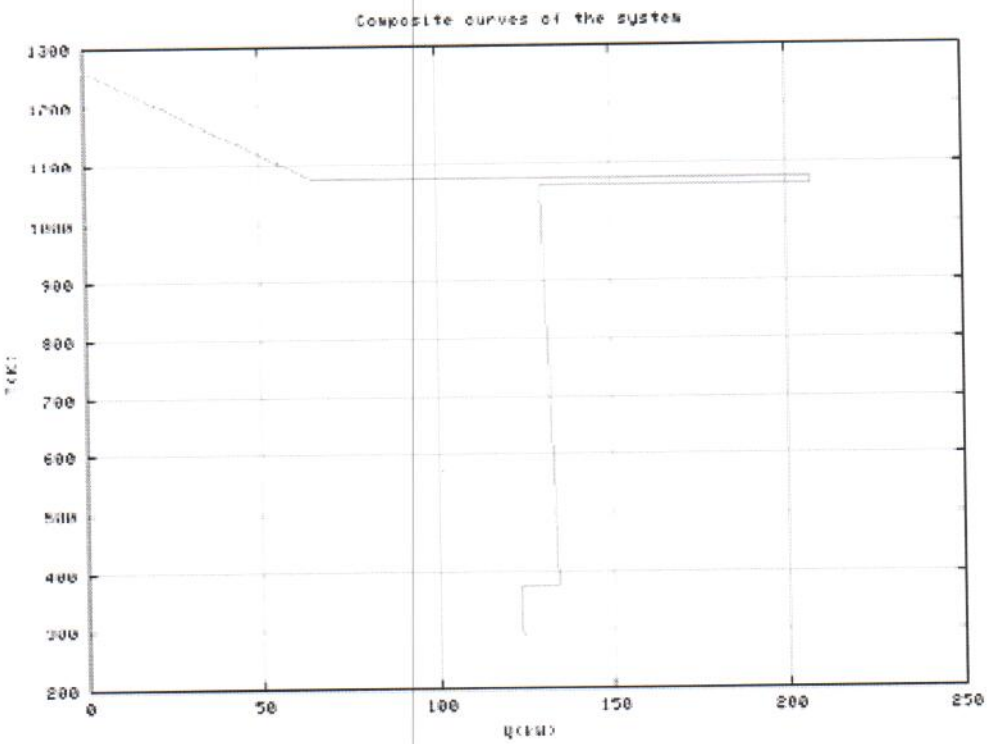

Fig. 12 : Grand composite curve, or difference between hot and cold composite curve of Fig. 11, of the SOFC biogas system, showing available excess heat at high temperature level (800°C).

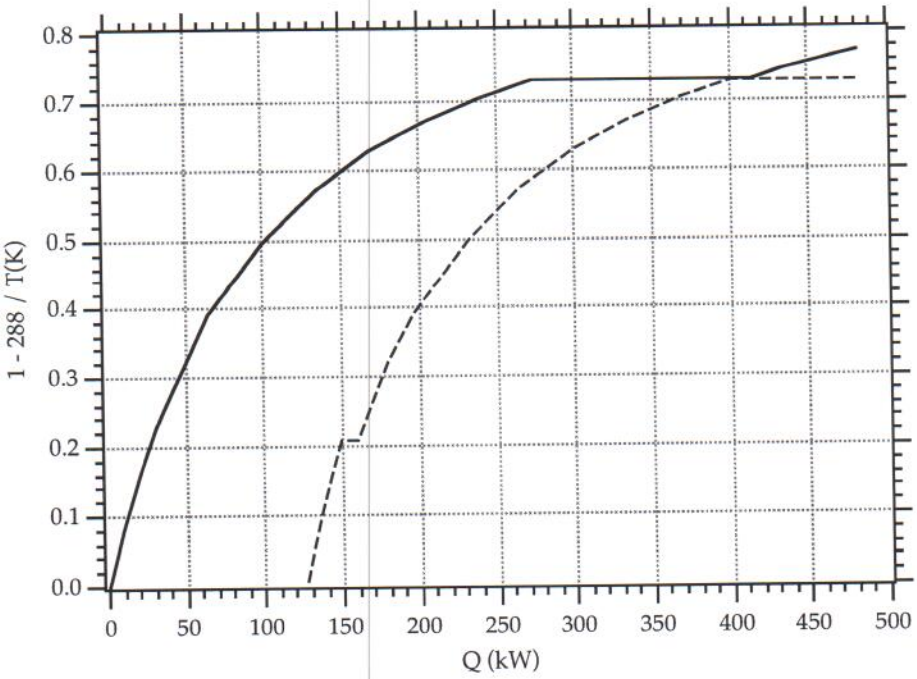

Fig. 13 : Exergy hot (upper) and cold (lower) composite curves of the SOFC-biogas system.

Fig. 13 finally shows another alternative to Fig.11, now plotted with the exergy equivalent on the Y-axis instead of absolute temperature. The factor (1-288 K/T(K)) corresponds to the Carnot efficiency factor for converting heat, between the two temperature levels T and T_0 (288 K, the environment), into work. The zone in between both exergy composite curves indicates all exergy loss occurring in internal heat exchange, if the present configuration of the system were to be maintained as such. In other words, the diagramme shows the potential for improved heat exchange within the system, that could be achieved when approaching both curves as closely as possible. This would require further close investigation of the physical layout of the various heat exchanges taking place, attributing appropriate exchange areas and transfer coefficients for each case. This will be reported in a forthcoming study.

4.4. Operating parameter sensistivity

Variable load

SOFC stack behaviour with variable biogas input flow is discussed in the following. At the outset, a constant flow of 43 m^3/h (design point) was postulated, in reality this input flow may fluctuate according to demand for electricity or heat or else according to biogas production availability. Results for a variable load, i.e. for changing biogas input flow between 20% to 200% of the design value, are given in Figs. 14 and 15. Fig. 14 shows quantitatively how electrical efficiency drops (between 61% and 37%) with increasing load, due to higher current density on the cells (up to 0.48 A/cm^2) at lower operating voltage (down to 0.51 V per cell). In effect, we move up and down the stack i-V curve when changing the fuel flow, while keeping the conversion (80%) constant. Fig. 15 shows that the electrical output between 20% and 200% fuel load varies from 30 kW to 205 kW (design point = 131 kW). At the same time, even though air excess λ has been kept constant (λ=3), i.e cathode air increases concomitantly when fuel input increases, the thermal gradient on the stack also increases, from the maximum tolerable 200 K between outlet and inlet at design point (131 kW, 100% load) to for example 250 K when running at 150% load (65 m^3 biogas/h). In other words, λ should be further increased at higher load and may be decreased at partial load.

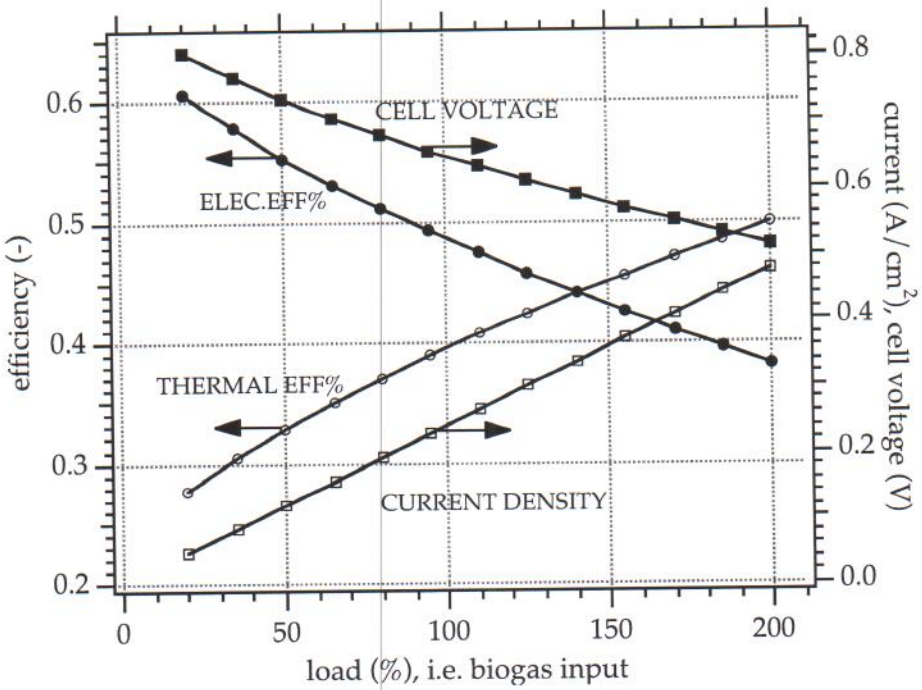

Fig. 14 : SOFC stack behaviour (efficiency, i-V) as a function of changing biogas input flow (20% to 200% of the design point 43 m^3/h). Electrical efficiency raises at partial load and drops at higher load.

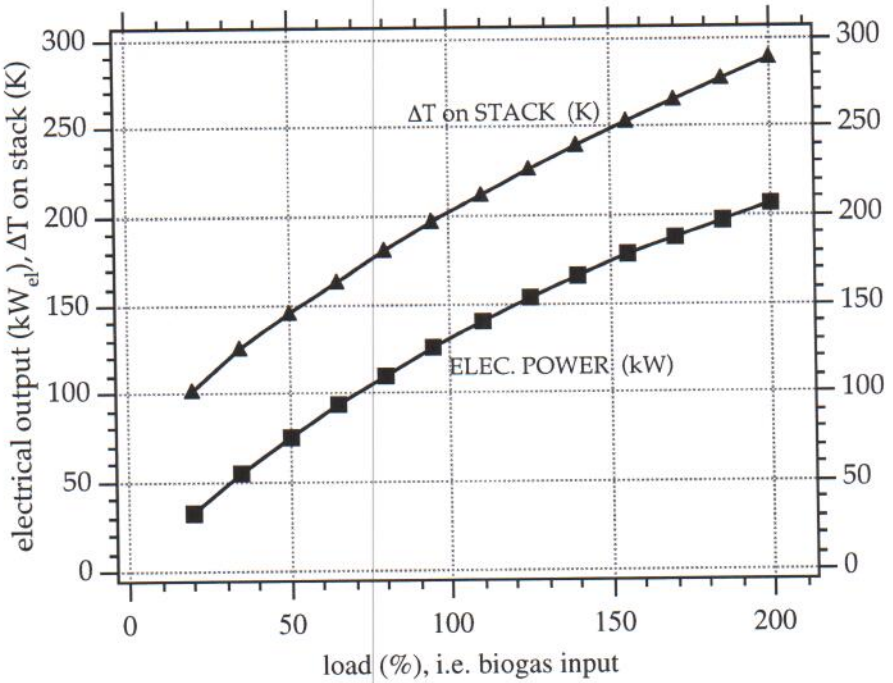

Fig. 15 : SOFC stack output and thermal gradient as a function of changing biogas input flow (20% to 200% of the design point 43 m^3/h). Power increase is not linear and thermal stress increases at higher load.

Fuel composition

The final graphs illustrate the effect of fuel composition variation at constant fuel inlet flow (43 m^3/h), either by changing the reforming steam level (S/C-ratio) or by fluctuations in the biogas CO_2 content. While the composition of sewage biogas is stable (Table 1), making it one of its attractive features, the composition of other biogas production sites may fluctuate strongly. Fig. 16 shows examples of this, the first (a) was measured on a 200 kW solid green waste methanisation plant (23), the second (b) was measured on a 10 kW farm waste digestion installation (23). In the first case, connected engines will stop functioning once the methane-level drops below 50%, which occurs periodically. This would not apply to a fuel cell. In the second case, important transients are periodically observed (air entry due to batch-refilling of the digesters) causing a simultaneous drop in methane and CO_2 levels.

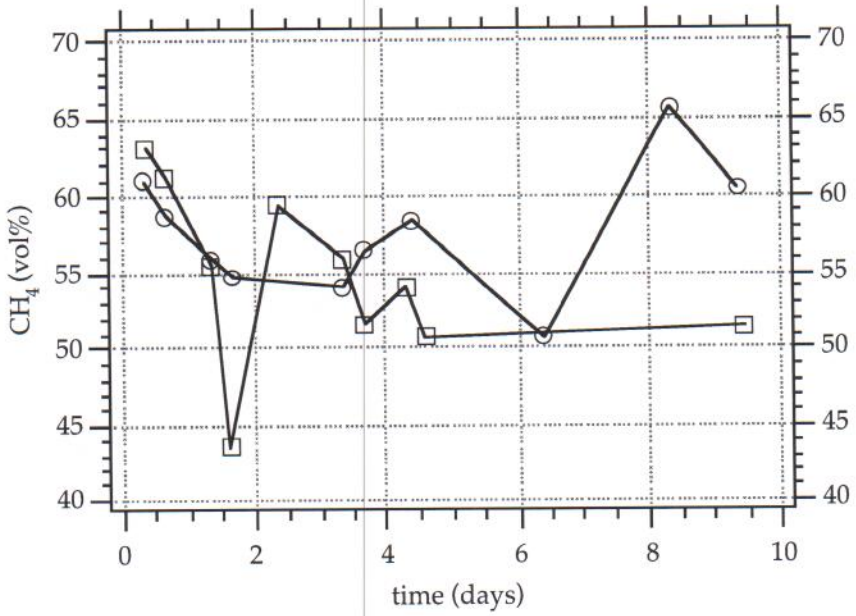

Fig. 16a : CH_4 content measured in biogas from a 200 kW methanisation plant of solid green waste, during 2 different 10-day periods (Nov 2002, Feb 2003).

Fig. 17 illustrates that an increasing CO_2 level in the biogas stream at constant flow rate obviously decreases power generation on the SOFC stack (by -2 kW_{el} per 1%-point increase in CO_2), but at the same time that efficiency slightly increases. As fuel conversion is constant (80%), less methane at

the inlet corresponds to smaller current density on the same stack and hence, moving up the i-V curve, to higher operating voltage and efficiency.

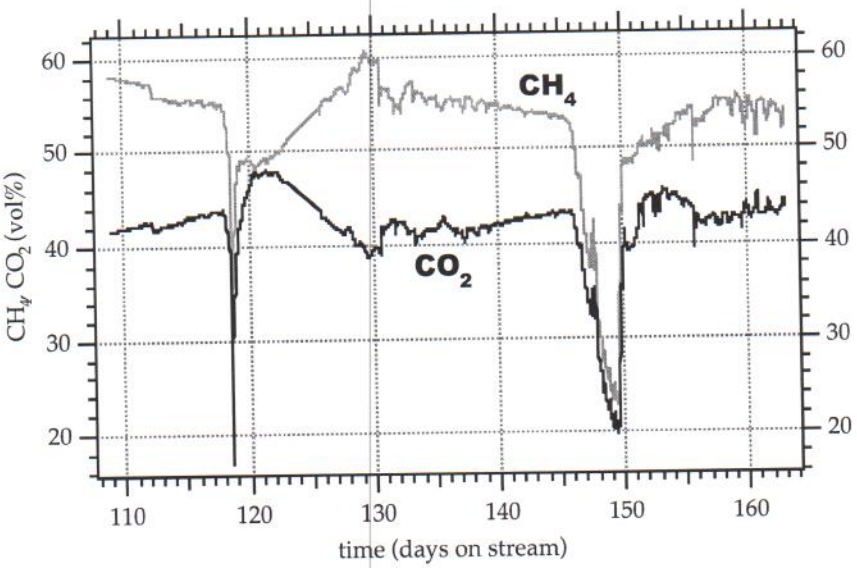

Fig. 16a : CH_4 and CO_2 content measured in biogas from a 10 kW farm waste digester during a one year test.

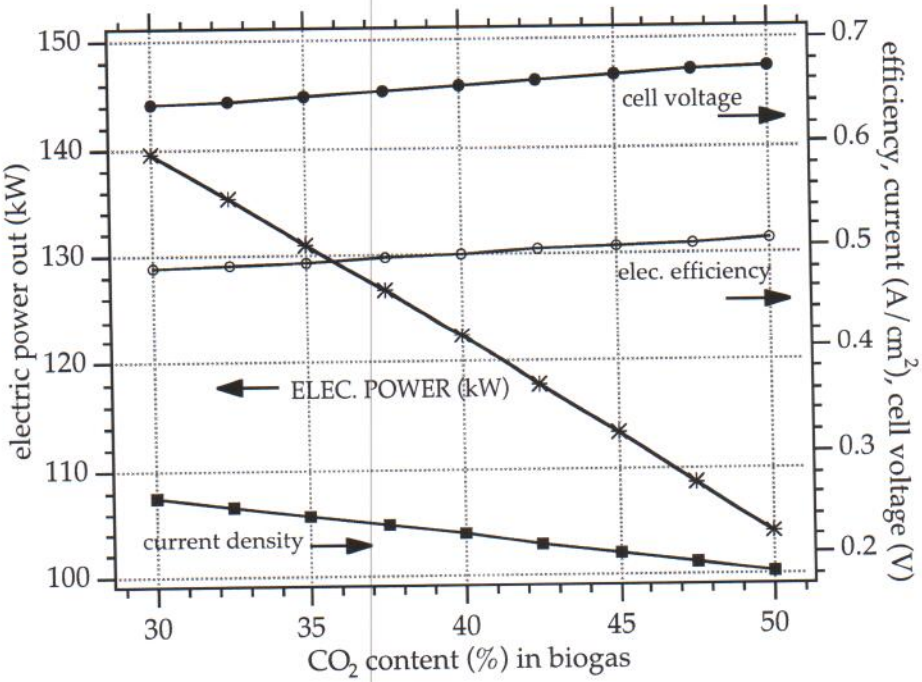

Fig. 17 : Variation of generated stack power and efficiency with the CO_2-level in the biogas feed, at constant flowrate. Power varies by about 2 kW_e per % variation in CO_2, and efficiency slightly drops for richer fuel as current density (constant conversion, 80%) then increases.

Fig. 18 shows the effect of further steam addition to the reformer. Doubling the steam amount (S/C=1) of the design value (S/C=0.5), and therefore almost excluding carbon formation anywhere in the system (Fig. 4), lowers the electrical output (from 131 to 127 kW) and efficiency (by 48.7 to 47%) by only a small amount. While current density remains constant, cell voltage does slightly drop owing to higher pH_2O at the anode. However, thermal efficiency also drops (from 39.7 to 36%), due to lower postcombustion temperature and higher steam preheating requirement, to a total cogeneration HHV efficiency of 83% (compared to 89% at design point, S/C=0.5).

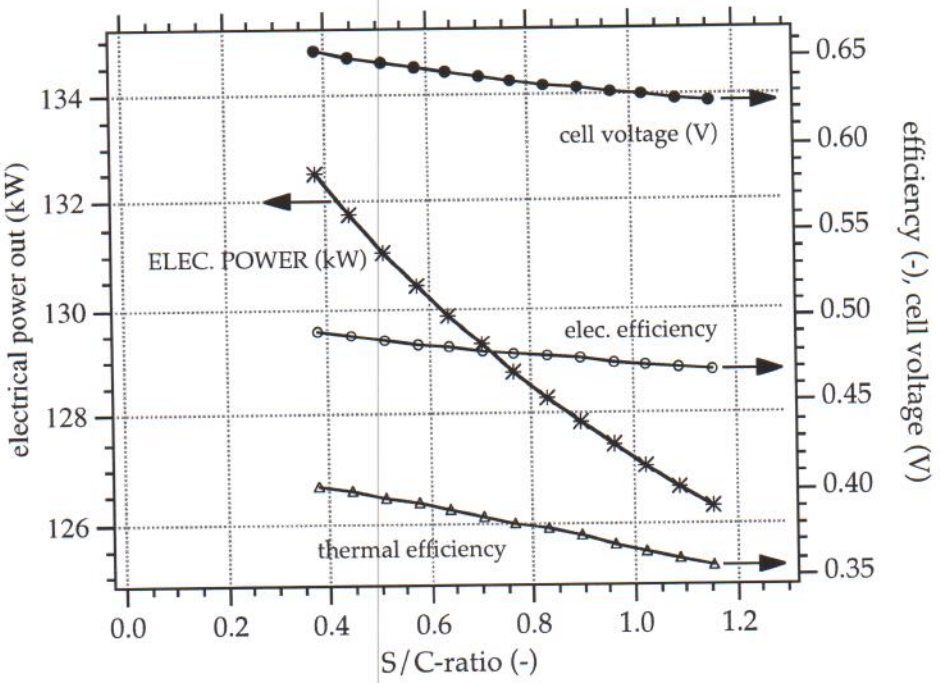

Fig. 18 : Variation of generated stack power and efficiency with S/C-ratio, both showing only a limited drop with the increase in added steam for reforming, due to a minor lowering in cell voltage (higher pH_2O at the anode).

For final evaluation, steam-reformed biogas was compared to a number of other input fuels or reforming conditions, maintaining the same system layout (Fig. 1) and electrochemical model. These are : steam-reformed pure methane, partially oxidized biogas, pure hydrogen and pure methane. The latter case is only hypothetical as severe carbon deposition would occur. It is included for theoretical reference purpose. In all cases, fuel flow was adjusted to give identical inputs of 269.3 kW everywhere. Table 5 summarizes the computed outputs. Steam reformed biogas is essentially

identical to steam-reformed methane; the CO_2 reforming compound inherent in biogas increases endothermal reformer cooling (78 kW vs. 71 kW), therefore upgrades the input fuel to a higher heating value at the reformer outlet, but this advantage is rather exactly compensated by an equivalent loss in the electrochemical reaction, CO oxidation being more entropic than H_2 oxidation (Q_{stack} 143 kW vs. 135 kW).

Partial oxidation (POX) reforming of the biogas obviously leads to lowered electrical efficiency (43%) due to partial fuel consumption already before entry to the stack. Cooling by the reformer, which approaches autothermal conditions, is far less (29 kW) and λ has to be increased from 3 to 4.5 to keep a similar thermal gradient of ca. 200 K between stack inlet and outlet. With H_2 fuel, the situation is similar to the case of partial oxidation, only cooling requirements are yet more extreme (λ=6) as no heat is evacuated through reforming. For the hypothetical direct methane fed system, finally, an ultimate theoretical HHV efficiency of 57% is found. Heat generation on the stack is very low (44 kW) and ΔT maintained at 200 K for an air excess λ equal to 2.

Table 5 : Comparison of stack output for different fuel processing methods and different fuel feeds

Parameter	Unit	Biogas steam-ref.	Biogas-pox	CH_4 steam-ref.	H_2	CH_4
steam-to-carbon ratio	-	0.5	-	1.15	-	-
O_2-to-CH_4 ratio	-	-	0.3	-	-	-
cell voltage	V	0.648	0.682	0.654	0.697	0.765
current density	A/cm^2	0.239	0.203	0.239	0.198	0.239
gross electric power	kW_{el}	134.2	120.3	135.4	119.6	154.6
air compressor power	kW_{el}	2.99	4.32	2.98	4.94	1.99
net electric power	kW_{el}	131.1	115.65	132.29	114.3	152.6
gross elec. efficiency	%	49.84	44.67	50.35	44.55	57.52
net elec. efficiency	%	48.66	42.94	49.20	42.58	56.74
thermal efficiency	%	39.58	46.36	36.98	45.63	38.40
stack generated heat	kW	142.9	117.9	135.4	101.2	44.3
reformer cooling power	kW	78.2	29.4	71.1	-	-
air excess λ	-	3	4.5	3	6	2
stack cooling air	kW	64.1	92.9	64.0	106.5	42.7
deltaT	K	202	191	201	190	207
hot exhaust	kW	318.0	411.0	313.2	437.1	230.2
cold exhaust loss	kW	20.4	29.1	20.2	31.8	13.2
postcombustion temperature	°C	987	915	987	897	1085

Conclusion

A 100 kW class SOFC system operated on biogas from sewage sludge digestion was defined in a process flow environment. Real data from an existing sewage plant was used as input : 43 m^3/h flow of biogas containing 63% CH_4 and 35% CO_2. Using reforming with added steam in a proportion appropriate to avoid carbon formation (S/C = 0.5), power generation from 269 kW input methane was 131 kW (48.7 % efficiency). Fuel conversion was set to 80% and minimal cell voltage to 0.65 V, requiring 2400 cells of 20 x 20 cm (361 cm^2 active area each) for the stack. Cooling of the stack was illustrated to be achievable to roughly equal parts by reforming and cathode air flow excess (λ=3). Thermal efficiency was almost 40% for total efficiency of 88.5%.

Hot and cold composite curves and exergy curves of the system indicate further improvement potential in internal heat exchange and high grade heat exploitation from stack and afterburner. This will be explored in further study.

The biogas-steam fuel behaved essentially identically to steam-reformed methane. Using partial oxidation of biogas, electrical efficiency drops to under 43% while λ needs to be raised to 4.5 to maintain a tolerable 200 K thermal gradient over the stack.

Acknowledgements

The company BELSIM (Liège, Belgium) is acknowledged for license use of the VALI data reconciliation software package. The Swiss Federal Energy Office is gratefully acknowledged for financial support (contract 79385). Special thanks to ERM, in particular M. A. Jotterand, the exploitation organisation of the sewage water treatment plant in Morges (VD), Switzerland, for providing the site production data and the biogas samples for analysis.

References

1. J. Van herle, Y. Membrez, O. Bucheli, *J. Power Sources*, accepted, in press (2003). Biogas as a fuel source for solid oxide fuel cell cogenerators.
2. M. Jenne, T. Zähringer, A. Schuler, G. Piskay and D. Moos, Proceedings of the 5th European Solid Oxide Fuel Cell Forum, U. Bossel ed., Lucerne, Switzerland, July 2002, European Forum Secretariat, CH 5452-Oberrohrdorf, Switzerland, p. 460-466. Sulzer HEXIS SOFC systems for biogas and heating oil.
3. http://www.fct.ca
4. S.C. Singhal, Proceedings of the 6th International Symposium on Solid Oxide Fuel Cells, Electrochemical Society Proceedings Series Vol 99-19, Honolulu, USA, Nov 1999, p.39-51. Progress in tubular SOFC technology.
5. L. Blum, L.G.J. de Haart, I.C. Vinke, D. Stolten, H-P. Buchkremer, F. Tietz, G.Blass, D. Stöver, J. Remmel, A. Cramer, R. Sievering, Proceedings of the 5th European Solid Oxide Fuel Cell Forum, U. Bossel ed., Lucerne, Switzerland, July 2002, European Forum Secretariat, CH 5452-Oberrohrdorf, Switzerland, p. 784-790. Planar Anode Substrate Type SOFC kW-class stack development,
6. J. Van herle, F. Maréchal, S. Leuenberger, D. Favrat, J. Power Sources 118 (2003) 375-383. Energy Balance Model of a SOFC cogenerator operated with biogas.
7. A. Solheim, in Final Report on SOFC Micromodelling, IEA Annex II Programme of R, D & D on Advanced Fuel Cells, published by the Swiss Federal Office of Energy, CH-3003 Bern, Switzerland, May 1992, pp. 9-21. Gas diffusion in pores.
8. C.H. Hamann, W. Vielstich, Elektrochemie II, Elektrodenprozesse, Angewandte Elektrochemie, Verlag Chemie, GmbH, D-6940 Weinheim, Germany, 1981, p.53.
9. S.C. Singhal, Proceedings of the 5th International Symposium on Solid Oxide Fuel Cells, Electrochemical Society Proceedings Series Vol 97-40, Aachen, Germany, June 1997, p. 37-50. Recent progress in tubular SOFC technology.
10. A. Khandkar, S. Elangovan, J. Hartvigsen, D. Rowley, R. Privette, M. Tharp, Proceedings of the 6th International Symposium on Solid Oxide Fuel Cells, Electrochemical Society

Proceedings Series Vol 99-19, SOFC VI, Honolulu, USA, Nov 1999, p.88-94. Status and progress in SOFCo's planar SOFC development.

11. R. Barfod, S. Koch, Y-L. Liu, P.H.Larsen, P.V.Hendriksen, Proceedings of the 8th International Symposium on Solid Oxide Fuel Cells, Electrochemical Society Proceedings Series Vol 2003-07, Paris, April 2003, p.1158-1167. Long term tests of DK-SOFC cells.
12. J. Van herle, Postgraduate Master Thesis in Energy Technology, Ecole Polytechnique Fédérale de Lausanne (EPFL), CH-1015 Lausanne, Switzerland, February 2001. SOFCs supplied with biogas.
13. J-L. Hersener, U. Meier, Swiss Federal Energy Office Report, CH-3003 Bern, Switzerland, April 1999. Energetisch nutzbares Biomassepotential in der Schweiz sowie Stand der Nutzung in ausgewaehlten EU-Staaten und den USA.
14. H. Verbockhaven, S. Loiseau, V. Blanchot-Courtois, Proceedings of the 3rd European Solid Oxide Fuel Cell Forum, ed. Ph. Stevens, Nantes, France, June 1998, European Forum Secretariat, CH 5452-Oberrohrdorf, Switzerland, p. 507-516. Evaluation of natural gas fueled SOFC for combined heat and power generation.
15. P. H. Middleton, M.E. Seiersten, B.C.H. Steele, Proceedings of the 1st International Symposium on Solid Oxide Fuel Cells, S.C. Singhal ed., Electrochemical Society Proceedings Series Vol 89-11, Florida, Nov 1989, p. 90-98.
16. M. Molinelli, D. Larrain, R. Ihringer, L. Constantin, N. Autissier, O. Bucheli, D. Favrat and J. Van herle, Proceedings of the 8th International Symposium on Solid Oxide Fuel Cells, Electrochemical Society Proceedings Series Vol 2003-07, SOFC VIII, Paris, April 2003, p.905-913. Current collection and stacking of anode support cells with metal interconnects to compact repeating units.
17. A. de Groot, N. Woudstra, J. Inst. of Energy 68 (3 1995), pp. 32-39. Exergy Analysis of a fuel cell system.
18. S.H. Chan, C.F. Low, O.L. Ding, J. Power Sources 103 (2002) 188-200. Energy and exergy analysis of simple SOFC power systems.
19. S. Linderoth, P.V. Hendriksen, M. Mogensen, N. Langvad, J. Mat. Sci 31, 5077-82 (1996). Investigations of metallic alloys for use as interconnects in SOFC stacks.

20. F.L. Lowrie, R.D. Rawlings, J. Eur. Ceram. Soc. 20 (2000) 751-706. Room and high temperature failure mechanisms in solid oxide fuel cell electrolytes.

21. D. Stolten, D. Froning, L. de Haart, Proceedings of the 4th European Solid Oxide Fuel Cell Forum, U. Bossel ed., Lucerne, Switzerland, July 2002, European Forum Secretariat, CH 5452-Oberrohrdorf, Switzerland, p. 347-356. Modeling of planar anode-supported thin YSZ layer SOFC stacks.

22. K. Honegger, A. Plas, Proceedings of the 7th International Symposium on Solid Oxide Fuel Cells, Electrochemical Society Proceedings Series Vol 2001-16, Tsukuba, Japan, June 2001, p.803-810. Evaluation of ferritic steel interconnects for SOFC stacks.

23. J. Van herle, Final report on Analysis of Biogas for Solid Oxide Fuel Cells for the Swiss Federal Energy Office, May 2003, CH-3003 Bern, Switzerland.